SAND89-1889C
Proposed for presentation at the
Lasers '89 Conference
12/3-8/89, New Orleans, LA

CONF-891261--1

Gasdynamic Phenomena in Nuclear-Reactor-Pumped Lasers

J. R. Torczynski
Sandia National Laboratories
Albuquerque, NM 87185-5800

SAND--89-1889C
DE90 005428

Abstract

In nuclear-reactor-pumped lasers, the fission-fragment heating is spatially nonuniform and as such induces gas motion. The competing effects of heating nonuniformity and thermal conduction on overall gas motion and laser optical behavior are examined, and a parameter is developed which categorizes the induced gas flow into three regimes. The effect of fission-fragment heating on perturbations in the gas density field is also examined, and a scaling relation describing the reduction of the rms density perturbation is developed in terms of the pressure rise produced by the heating.

This work was performed at Sandia National Laboratories, supported by the U. S. Department of Energy under contract number DE-AC04-76DP00789.

---

1. Introduction

Fragments from fission reactions induced by a pulse of neutrons from a nuclear reactor have been used to pump a variety of gas lasers.[1–10] These "nuclear-reactor-pumped" lasers offer several advantages over more conventional pumping schemes. First, the fission-fragment energy is used to excite atomic or molecular lasing states directly, rather than first being converted to heat, electricity, and possibly light with the attendant efficiency losses.[11] Second, the large power density associated with nuclear power implies a compact power source.[11]

Figure 1 shows a schematic diagram of one possible arrangement. The reactor serves as the source of fast neutrons, which are moderated by polyethylene. The resulting slow neutrons are incident on thin layers of fissionable material (coating the inner surfaces of the laser gas cell), which emit fission fragments into the adjacent gas. These fission fragments pump the lasing states and heat the gas. One difficulty in this approach is evident from Figure 1. The fission fragments enter the gas from the side walls in this arrangement and heat the gas in these regions more strongly than they heat the gas near the optical axis. This heating nonuniformity induces an inward flow and establishes density gradients perpendicular to the optical axis. Since gradients of the gas density are proportional to gradients of the refractive index, the laser gas acts as a temporally varying gradient-index lens. This gasdynamic lensing can be of strength sufficient to induce transitions in laser resonator stability (see Figure 2).[12–14]

In this paper, the effects of fission-fragment heating on the gas density field are examined. First, the overall gas motion resulting from the spatial nonuniformity of fission-fragment heating is studied, and the resulting flows are characterized in terms of the ratio of the duration of the heating to the thermal-conduction timescale. Second, the effect of fission-fragment heating on small perturbations in the gas density field is analyzed. The density-dependence of fission-fragment heating is shown to result in a damping of density perturbations. This damping is seen to be relatively broadband, and a scaling relation is developed for the reduction of the rms density perturbation level.

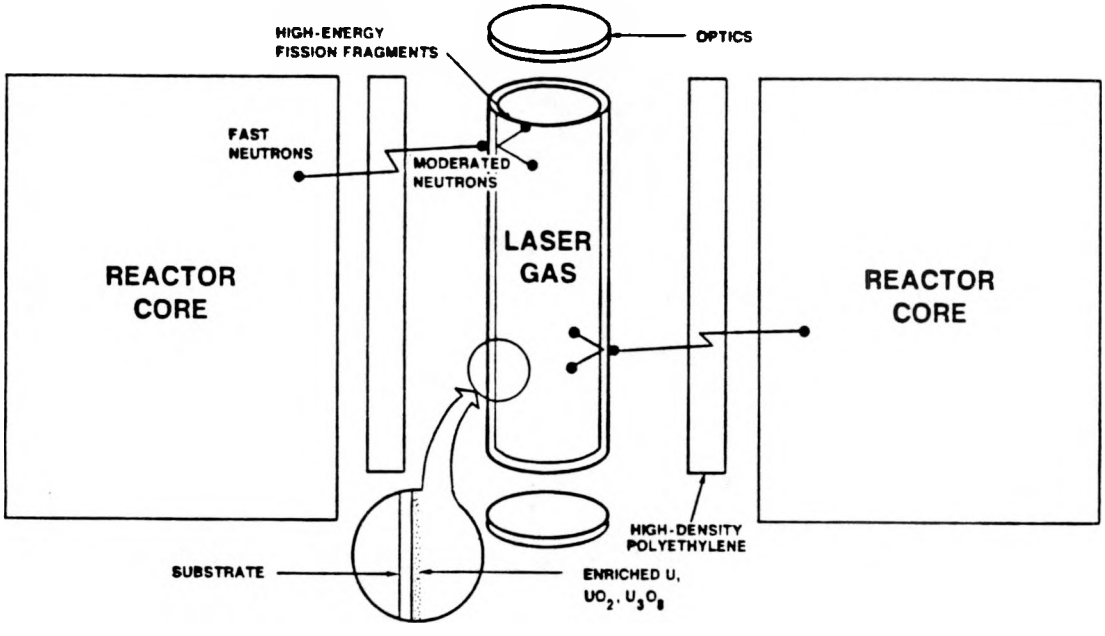

Figure 1. Schematic diagram of a nuclear-reactor-pumped laser experiment.

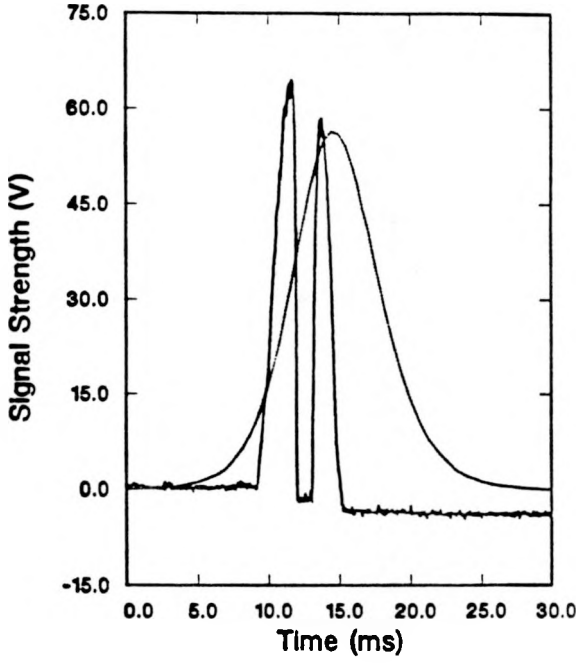

Figure 2. Lasing intensity (solid curve) and pumping pulse (dotted curve). Resonator stability transitions induced by gasdynamic lensing result in the lasing termination and reinitiation seen at 12 ms and 13 ms, respectively (peak pumping is at 15 ms).

2. The Model Problem

A diagram of a typical laser cell is shown in Figure 3. The geometry here is rectangular, rather than cylindrical as in Figure 1. Since the fissionable material is located on the two side walls normal to the x-axis, the heating nonuniformity induces flow in the x-direction. Although there are heating nonuniformities in the y- and z-directions that also induce gas motion, these nonuniformities are usually minor compared to the nonuniformity in the x-direction and are neglected in this study.

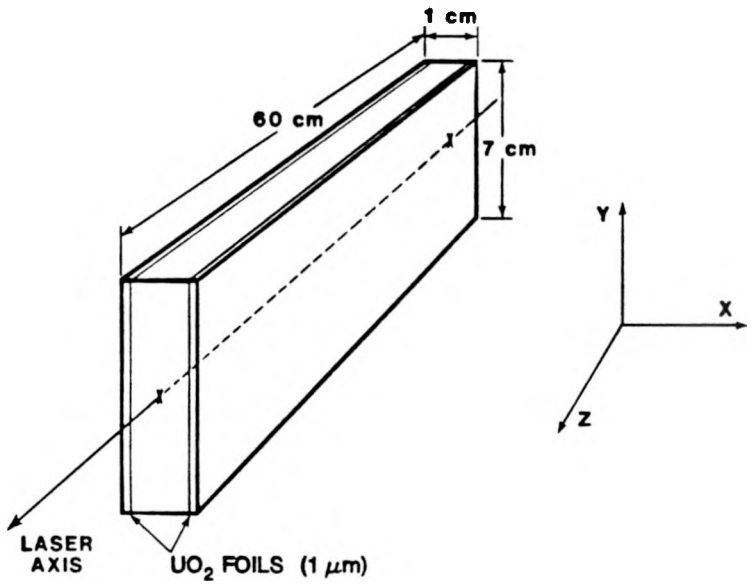

Figure 3. Diagram of a rectangular nuclear-reactor-pumped laser cell.

The gas in the laser cell is taken to be a mixture of perfect gases with nonzero shear and bulk viscosities and thermal conductivity. Its motion is governed by the conservation equations for mass, momentum, and energy, in which variations are permitted only in time and in the x-direction (see the appendix). At the side walls, the gas velocity is assumed to vanish, and the gas temperature is taken to be the wall temperature (presumed to be the initial gas temperature). Fission-fragment heating appears in the energy equation as a large,

transient, volumetric energy source term. This source term has the form $Q = Q_0 f[x;\rho]\, h(t)$, where Q_0 is the amplitude of the pumping, $h(t)$ is the time variation of the neutron flux and hence the heating, and $f[x;\rho]$ is the spatial variation of the heating. Figure 4 indicates the general forms of the functions f and h. The precise shape of the function f depends on the density field ρ since the gas molecules are essentially absorbers.[15-18] If the density field is made to vary in the laser cell, this variation in the distribution of absorbers produces a corresponding change in the function f: where the number of absorbers is increased, f is increased, and where the number of absorbers is decreased, f is decreased. Thus, gas motion and fission-fragment heating are coupled.[18]

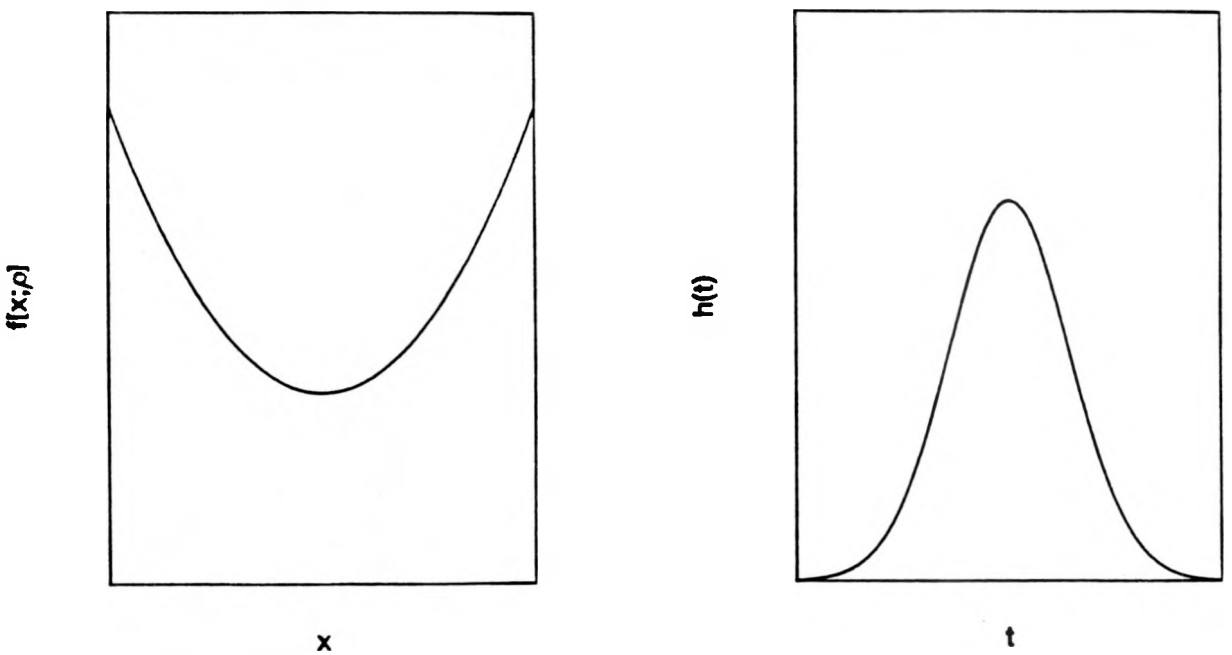

Figure 4. The spatial variation of fission-fragment heating is shown on the left. It is largest near the side walls and smallest near the center. The temporal variation of fission-fragment heating is shown on the right.

The combination of fission-fragment heating and thermal-conduction loss induces a flow that moves gas toward the "coldest" spots and away from the "hottest" spots.[19] Here, the term "coldest" indicates the regions where the sum of the fission-fragment heating and thermal-conduction loss is smallest (most negative), and similarly the term "hottest" indi-

cates the regions where the sum of fission-fragment heating and thermal-conduction loss is largest (most positive). This points out an interesting aspect of the induced flow. Fission-fragment heating is largest near the side walls and smallest at the center (see Figure 4); therefore, fission-fragment heating acts to induce flow inward toward the center. Thermal-conduction effects are most negative near the cold side walls and vanish near the center; therefore, thermal-conduction effects act to induce flow outward away from the center. Thus, the effects of heating nonuniformity and thermal conduction are oppositely directed, so the type of flow that results is determined by whichever effect is stronger.[19]

3. Gas-Flow Regimes

There are four timescales involved in describing the induced gas motion: t_A, the time required for an acoustic wave to travel from the center to the side walls; t_C, the time required for heat to be conducted from the center to the side walls; t_D, the duration of the heating (see Figure 4); and t_Q, the time required for the fission-fragment heating to raise the pressure by an amount comparable to the initial gas pressure. For conditions of interest, the acoustic timescale t_A is much smaller than the other three timescales. Because of this, the equations of motion can be acoustically filtered,[18-22] and the timescale t_A does not enter the resulting equations (the acoustically filtered equations are contained in the appendix).

Of the remaining three timescales, two dimensionless ratios may be formed. The ratio t_D/t_Q sets the scale, relative to the initial gas pressure, for the pressure rise induced by fission-fragment heating. The ratio t_D/t_C determines the flow type and is given by the relation

$$\frac{t_D}{t_C} \approx \frac{16(\gamma-1)k_0T_0t_D}{p_0L^2} , \tag{1}$$

where γ is the specific heat ratio of the gas, k_0 the initial thermal conductivity of the gas, T_0 the initial gas temperature, p_0 the initial gas pressure, and L the distance between the side walls. As such, t_D/t_C can be interpreted as a normalized thermal conductivity, so the magnitude of t_D/t_C determines the importance of thermal conduction over the duration of

the pulse. Three distinct regimes of flow behavior are possible depending on the magnitude of t_D/t_C. In the negligible-conduction regime ($t_D/t_C \ll 1$), the flow is dominated by the spatial variation of the fission-fragment heating. In the dominant-conduction regime ($t_D/t_C \gg 1$), the flow is dominated by thermal-conduction effects. In the mixed regime ($t_D/t_C \sim 1$), fission-fragment heating and thermal-conduction effects are of comparable importance.

3.1 Negligible-Conduction Regime

The negligible-conduction regime corresponds to conditions for which $t_D/t_C \ll 1$. An analytical solution exists in the limit that this ratio becomes vanishingly small.[18-19] From this solution, it is seen that gas moves inward from the side walls toward the center of the laser cell. This is as expected since the center is the "coldest" region in the absence of thermal-conduction effects. This inward gas flow creates a central maximum in the density field, so the laser cell is optically focusing. The uniformity of the fission-fragment heating is improved by this flow since gas molecules (absorbers) are transported out of regions of large heating near the side walls into regions of small heating near the center. Another fact that emerges from the analytical solution is that the added *energy*, not the applied heating *power*, determines the shape of the density profile. Consider two experiments identical in all particulars except that in one case the heating is applied at half the power but for twice the duration of the other case. Since the same amount of energy is added in both cases, the same density profile is produced in both cases.

As an example, consider helium, initially at 300 K and 200 kPa, confined between side walls separated by a 1-cm gap and coated with 1-μm UO_2 layers. A constant power density of 3550 W/cm^3 is used to heat the gas for 0.1 ms. These conditions correspond to a value of 0.0095 for t_D/t_C. Figure 5 shows results from a simulation of the acoustically filtered equations (not the limiting analytical solution). The central density maximum is clearly seen and continues to grow with increasing energy addition. Note the appearance of thin thermal boundary layers adjacent to the side walls. These result from the nonzero value

of t_D/t_C; nevertheless, the flow in the central region is relatively unaffected by thermal-conduction effects.

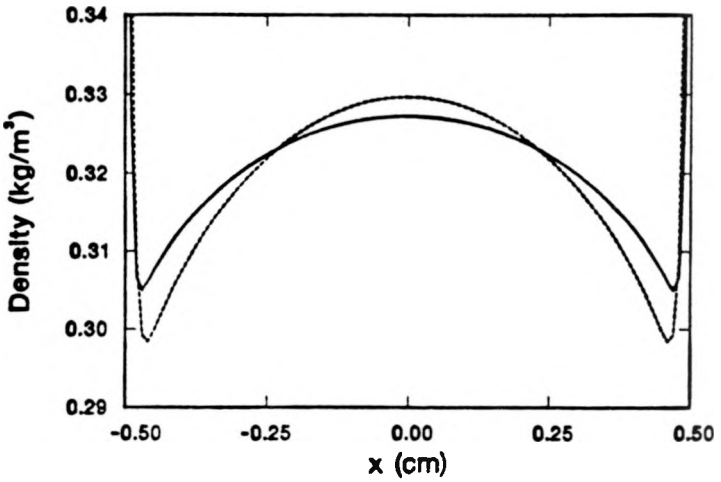

Figure 5. Density profile for a case in the negligible-conduction regime: solid curve, midway through the pulse; dashed curve, end of the pulse.

3.2 Dominant-Conduction Regime

The dominant-conduction regime corresponds to conditions for which $t_D/t_C \gg 1$. An analytical solution exists in the limit that this ratio becomes infinitely large.[19] From this solution, it is seen that gas moves outward from the center of the laser cell toward the side walls. This is as expected since the side walls are the "coldest" regions when thermal-conduction effects are very large. This outward gas flow creates a central minimum in the density field, so the laser cell is optically defocusing. The uniformity of the fission-fragment heating is degraded by this flow since gas molecules (absorbers) are transported out of regions of small heating near the center into regions of large heating near the side walls. Another fact that emerges from the analytical solution is that the applied heating *power*, not the

added *energy*, determines the shape of the density profile. If the applied heating power is held constant, the density profile does not change even though energy is continually added.

As an example, consider helium, initially at 300 K and 200 kPa, confined between side walls separated by a 1-cm gap and coated with 1-μm UO_2 layers. A constant power density of 2.22 W/cm^3 is used to heat the gas for 160 ms (these values differ by a factor of 1600 from the values used in the previous example but maintain the same energy addition). These conditions correspond to a value of 15 for t_D/t_C. Figure 6 shows results from a simulation of the acoustically filtered equations (not the limiting analytical solution). The central density minimum is clearly seen and does not change much with increasing energy addition. The slight changes in the density field with increasing energy addition is indicative of the finite value of t_D/t_C.

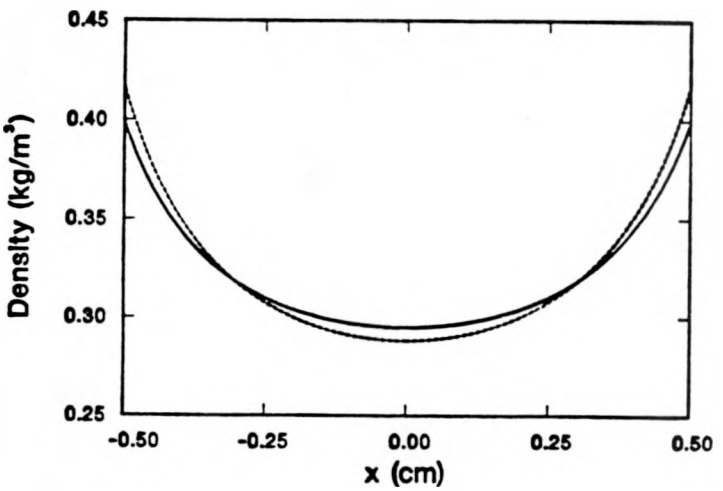

Figure 6. Density profile for a case in the dominant-conduction regime: solid curve, midway through the pulse; dashed curve, end of the pulse.

3.3 Mixed Regime

The mixed regime corresponds to conditions for which $t_D/t_C \sim 1$. Unfortunately no

analytical solution is known for this regime, so insight must be gleaned from numerical solutions for many different sets of conditions. The following observations can be made.[19] At early times in the pulse and for gas near the center, the motion resembles the negligible-conduction regime. However, at later times and for gas near the side walls, the motion resembles the dominant-conduction regime. Thus, the gas near the center moves toward the center, and the gas near the side walls moves toward the side walls. This complex gas motion creates a central density maximum and density minima propagating inward from the side walls toward the center, so both focusing and defocusing regions are present. Both the added energy and the applied heating power affect the gas motion in the mixed regime, and the uniformity of the fission-fragment heating is improved near the center but degraded near the walls.

As an example, consider helium, initially at 300 K and 200 kPa, confined between side walls separated by a 1-cm gap and coated with 1-μm UO_2 layers. A constant power density of 89 W/cm^3 is used to heat the gas for 4.0 ms (these values are the geometric means of the values used in the two previous examples and as such maintain the same energy addition). These conditions correspond to a value of 0.38 for t_D/t_C. Figure 7 shows results from a simulation of the acoustically filtered equations. The central density maximum and the density minima near the side walls are clearly seen. These minima travel noticeably inward during the pulse. Note that the curvature of the central density maximum remains relatively constant as the overall density falls in the central region. This phenomenon is often observed although it is not currently explained.

4. Density Perturbations

In the previous section, the effect of the combination of fission-fragment heating and thermal-conduction loss on the overall gas motion was considered. In this section, the effect of fission-fragment heating on small density perturbations is examined. Since density perturbations are hard to avoid and their presence generally exerts a detrimental effect on laser

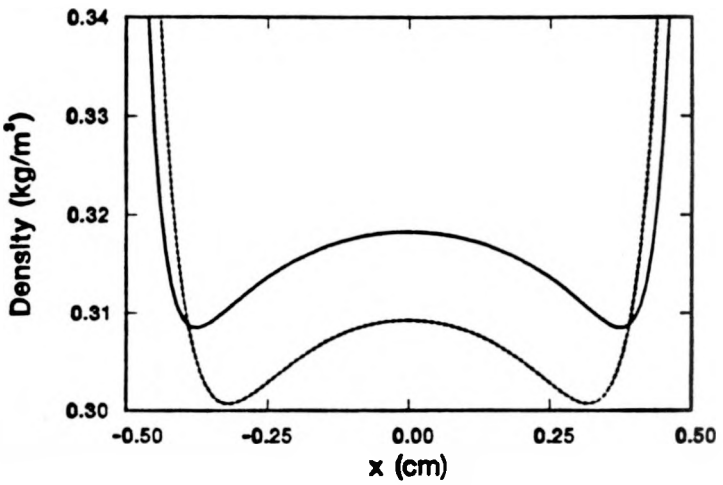

Figure 7. Density profile for a case in the mixed-conduction regime: solid curve, midway through the pulse; dashed curve, end of the pulse.

optical behavior, it is of interest to examine the interaction of fission-fragment heating with density perturbations, particularly regarding growth, damping, or lengthscale change.

The basic effect of fission-fragment heating on density perturbations is illustrated in Figure 8. This figure shows an expanded view of a small portion of the density profile which contains two density perturbations. The positive perturbation contains more gas molecules (absorbers) and is heated more strongly than surrounding regions of gas. This excess heating creates a slightly larger pressure in the perturbation than in neighboring regions, and this pressure difference acts to transport gas away from the perturbation, reducing its height. Similarly, the negative perturbation contains less gas molecules (absorbers) and is heated less strongly than surrounding regions of gas. This shortfall of heating creates a slightly lower pressure in the perturbation than in neighboring regions, and this pressure difference acts to transport gas toward the perturbation, reducing its depth. Thus, fission-fragment heating smooths out density perturbations.

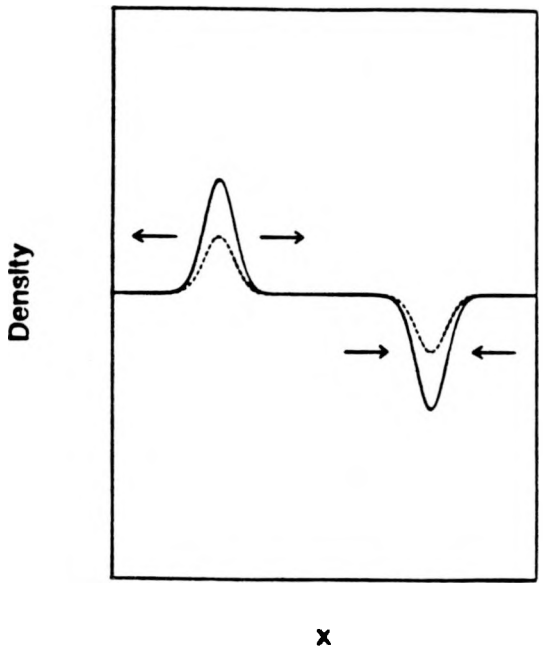

Figure 8. Expanded view of a small portion of the density profile (solid curve) with two density perturbations. These perturbations are smoothed (dashed curve) by fission-fragment heating. Arrows indicate the induced flow.

As an example, consider argon, initially at 300 K and 68.9 kPa, confined between side walls separated by a 1-cm gap and coated with 1-μm UO_2 layers. Figure 9 shows the evolution with increasing energy addition of two different initial density fields, one with perturbations and one without. To illustrate the role of fission-fragment heating in damping density perturbations, thermal-conduction effects have been suppressed, and artificially large density perturbations have been used for initial conditions (it is shown below that the perturbation amplitude does not matter). The inward flow of gas toward the center is evident for both the perturbed and unperturbed density fields. Moreover, the amplitude of the density perturbations is reduced with increasing energy addition. This fact is highlighted by Figure 10, which displays the difference between the perturbed and the unperturbed density fields for successive amounts of energy addition.

Careful scrutiny of Figure 10 reveals another aspect of the damping process. Both broad and narrow features exhibit the same amount of damping (for example, compare the broad feature near 0.42 cm to the narrow features near 0.38 cm). Figure 11 shows the evolution of two density profiles having perturbations with the same amplitudes but with wavelengths differing by a factor of 10. Note that both perturbations are contained within the same

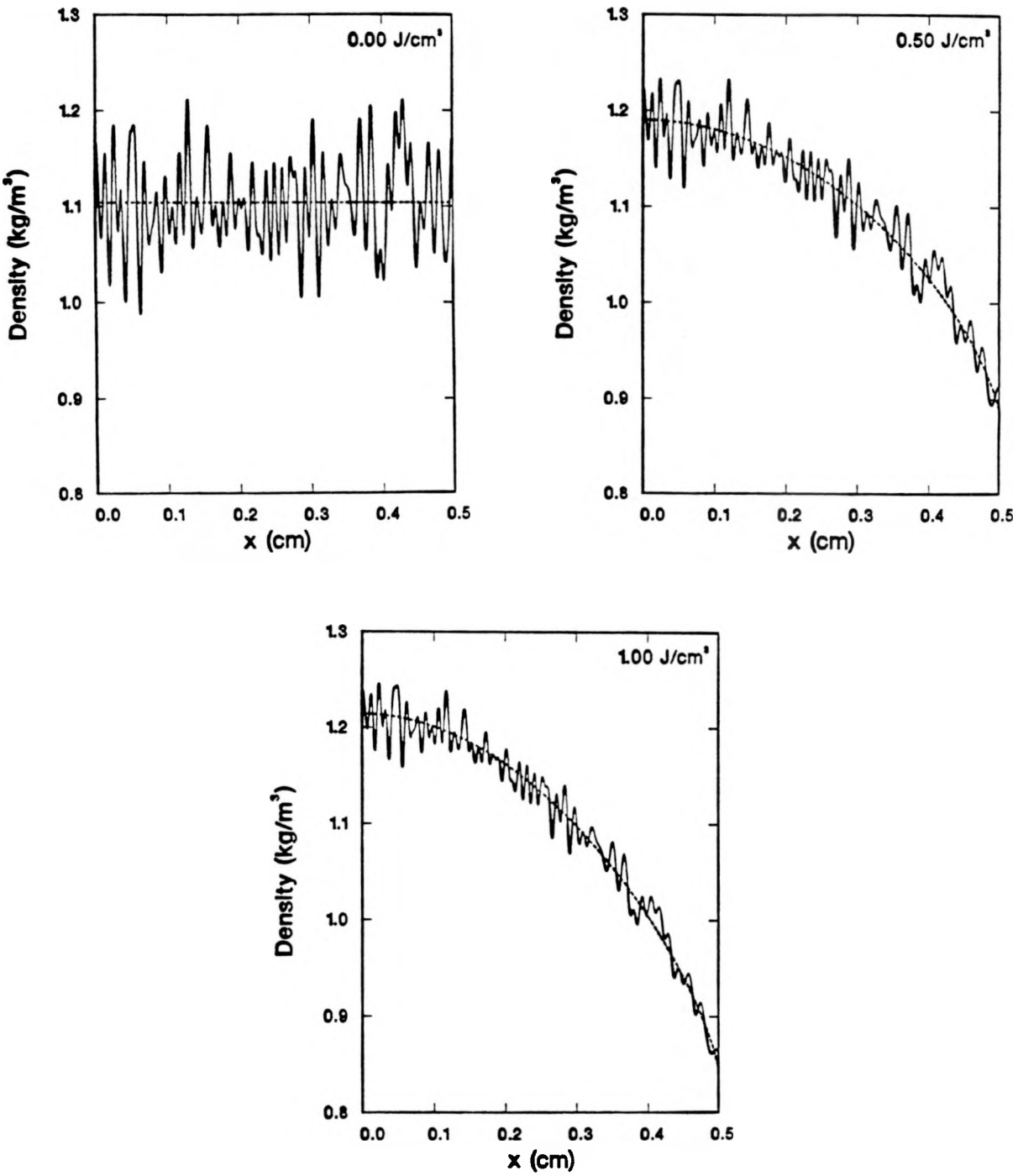

Figure 9. Density profiles at successive amounts of energy addition: solid curves, perturbed density field; dashed curves, unperturbed density field. Profiles are symmetric and thus are shown from center to wall, rather than from wall to wall.

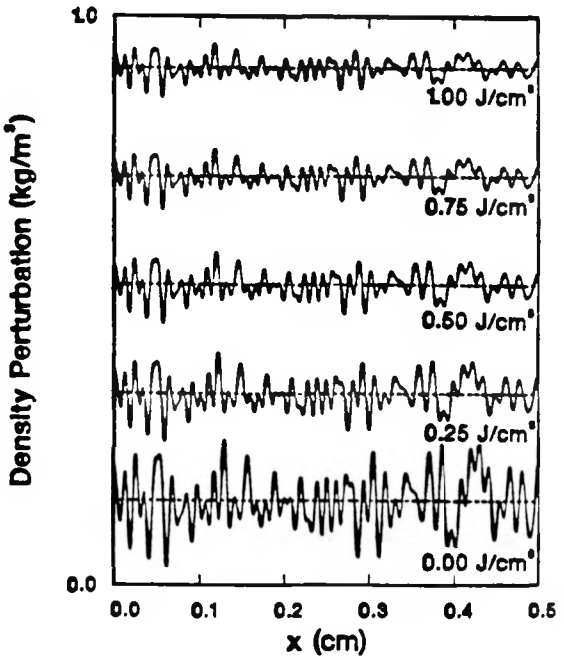

Figure 10. The density perturbation profiles (the difference between the perturbed and the unperturbed profiles) are shown as a function of energy addition.

envelope at successive values of energy addition. The damping is thus seen to be broadband and relatively insensitive to wavelength.

The broadband nature of the damping process suggests that it can be characterized in terms of the rms density perturbation,

$$\Delta\rho_{\rm rms} = \left[\frac{1}{L}\int_0^L (\rho - \rho_U)^2\, dx\right]^{1/2} , \tag{2}$$

where ρ is the perturbed density field and ρ_U is the unperturbed density field. The reduction in perturbation amplitude is given by $\Delta\rho_{\rm rms}/\Delta\rho_{\rm rms,0}$, where $\Delta\rho_{\rm rms,0}$ is the initial rms density perturbation. Simulations of different cases can be used to determine the manner in which this reduction varies with increasing energy addition. Table 1 shows the conditions of four such cases, and Figure 12 shows the reduction in terms of the quantity $(\bar{p}/p_0)^{1/\gamma}$. In this representation, the results all collapse onto one line with a slope of -1, so the following

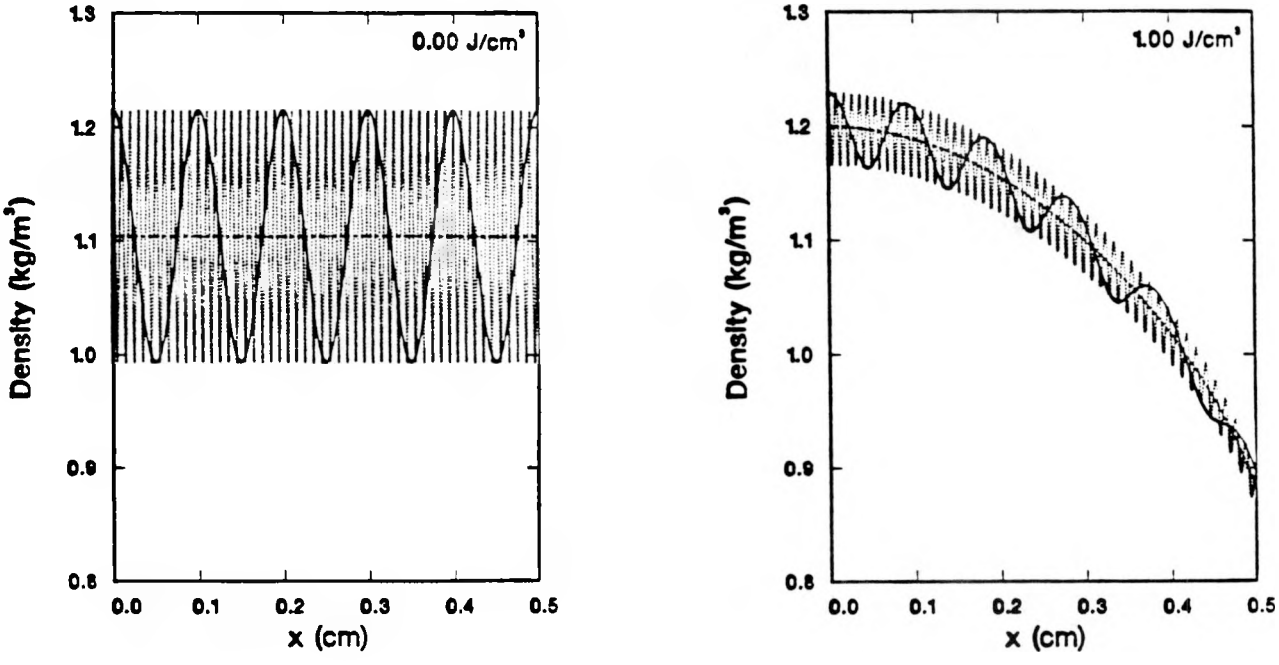

Figure 11. Two density profiles having perturbations with greatly differing wavelengths evolve in a similar fashion.

scaling relation is determined:

$$\frac{\Delta\rho_{\text{rms}}}{\Delta\rho_{\text{rms},0}} \approx \left(\frac{\bar{p}}{p_0}\right)^{-1/\gamma} . \tag{3}$$

If the perturbation amplitude is small compared with the initial gas density, the analytical solution for the negligible-conduction regime can be used to derive this result.[23] Note that this damping is algebraic in the pressure rise and thus requires large pressure rises to produce significant damping.

Table 1. Conditions for cases shown in Figure 12.

Symbol	p_{He} (kPa)	p_{Ar} (kPa)	T (K)	Gap L (cm)	UO_2 Thickness (μm)
△	0.0	68.9	300	1.0	1.0
▽	0.0	68.9	300	1.5	1.0
□	68.9	68.9	300	1.0	1.0
○	68.9	68.9	300	1.5	1.0

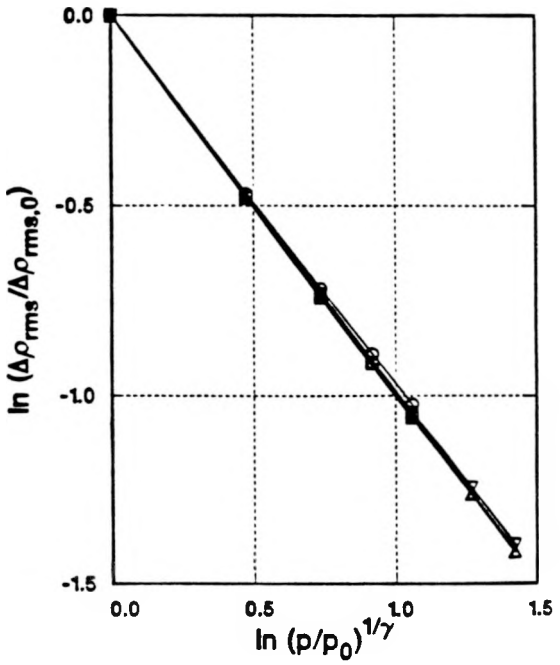

Figure 12. The quantity $\ln(\Delta\rho_{rms}/\rho_{rms,0})$ is plotted against $\ln(\bar{p}/p_0)^{1/\gamma}$ for a variety of different cases (see Table 1). The data exhibit a scaling relation.

5. Conclusions

The gas motion in nuclear-reactor-pumped lasers induced by fission-fragment heating has been examined. The spatial nonuniformity of fission-fragment heating induces a flow of gas toward the center of the laser cell, whereas thermal-conduction effects induce flow toward the side walls. Since these effects are oppositely directed, the type of flow that results is determined by whichever effect is stronger. The ratio of the heating duration to the thermal-conduction timescale, t_D/t_C, characterizes the importance of thermal-conduction effects, and the flow can be categorized into three regimes depending on the value of this ratio. If t_D/t_C is much less than unity, then the flow is in the negligible-conduction regime, in which a central density maximum is produced and the added energy determines the height of the maximum. If t_D/t_C is much greater than unity, then the flow is in the dominant-conduction regime, in which a central density minumum is produced and the applied heating power determines the depth of the minimum. If t_D/t_C is comparable to unity, then the flow is in the mixed

regime, in which both a central density maximum and density minima traveling inward from the side walls are produced and both the energy and the power influence the motion.

The density-dependence of fission-fragment heating is seen to result in damping of density perturbations. A scaling relation has been developed describing the reduction of the rms density perturbation in terms of the pressure rise produced by fission-fragment heating. This damping is broadband in the sense of being insensitive to the wavelength of the density perturbation. However, the algebraic nature of the scaling relation indicates that large pressure rises are required to produce significant damping.

Acknowledgments

The author gratefully acknowledges many discussions with Dan Neal, Joe Alford, Dave McArthur, Bill Sweatt, Bob Gross, Jim Rice, Paul Pickard, and Gerry Hays. This work was performed at Sandia National Laboratories, supported by the U. S. Department of Energy under contract number DE–AC04–76DP00789.

References

1. K. Thom and R. T. Schneider, "Nuclear Pumped Gas Lasers," *AIAA J.* **10**, 400–406 (1972).

2. D. A. McArthur and P. B. Tollefsrud, "Observation of Laser Action in CO Gas Excited Only by Fission Fragments," *Appl. Phys. Lett.* **26**, 187–190 (1975).

3. H. H. Helmick, J. L. Fuller, and R. T. Schneider, "Direct Nuclear Pumping of a Helium-Xenon Laser," *Appl. Phys. Lett.* **26**, 327–328 (1975).

4. G. H. Miley, "Direct Nuclear Pumped Lasers — Status and Potential Applications," in *Laser Interaction and Related Plasma Phenomena* **4**, edited by H. Hora and G. Miley (Plenum, New York, 1976), pp. 181–228.

5. M. A. Prelas, M. A. Akerman, F. P. Boody, and G. H. Miley, "A Direct Nuclear Pumped 1.45-μ Atomic Carbon Laser in Mixtures of He-CO and He-CO_2," *Appl. Phys. Lett.* **31**, 428–430 (1977).

6. R. J. De Young, Y. J. Shiu, and M. D. Williams, "Fission-Fragment Nuclear Lasing of Ar(He)-Xe," *Appl. Phys. Lett.* **37**, 679–6681 (1980).

7. A. M. Voinov, L. E. Dovbysh, V. N. Krivonosov, S. P. Mel'nikov, I. V. Podmoshenskii, and A. A. Sinyanskii, "Fission-Pumped He-Xe and Ar-Xe Infrared Lasers," *Sov. Tech. Phys. Lett.* **7**, 437 (1981).

8. G. N. Hays, D. A. McArthur, D. R. Neal, and J. K. Rice, "Gain Measurements Near 351 nm in $^3He/Xe/NF_3$ Mixtures Excited by Fragments from the $^3He(n,p)^3H$ Reaction," *Appl. Phys. Lett.* **49**, 363–365 (1986).

9. J. K. Rice, G. N. Hays, D. R. Neal, D. A. McArthur, and W. J. Alford, "Nuclear Reactor Excitation of XeF Laser Gas Mixtures," in *Proceedings of the International Conference on Lasers '86*, edited by R. W. McMillan (STS Press, McLean, VA, 1987), pp. 571–578.

10. D. A. McArthur, G. N. Hays, W. J. Alford, D. R. Neal, D. E. Bodette, and J. K. Rice, "Recent Results on Reactor-Pumped Laser Studies at Sandia National Laboratories," in *Laser Interaction and Related Plasma Phenomena* **8**, edited by H. Hora and G. Miley (Plenum, New York, 1988).

11. G. H. Miley, *Direct Conversion of Nuclear Radiation Energy* (American Nuclear Society, LaGrange, IL, 1970), Chaps. 3–4.

12. J. R. Torczynski and D. R. Neal, *Effect of Gasdynamics on Resonator Stability in Reactor-Pumped Lasers*, Sandia Report SAND88-1318, Sandia National Laboratories (1988).

13. D. R. Neal, J. R. Torczynski, and W. C. Sweatt, "Resonator Stability Effects in "Quadratic-Duct" Nuclear-Reactor-Pumped Lasers," in *Proceedings of the International Conference Lasers '88*, edited by R. C. Sze and F. J. Duarte (STS Press, McLean VA, 1989), pp. 245–252.

14. D. R. Neal, W. C. Sweatt, and J. R. Torczynski, "Resonator Design with an Intracavity Time-Varying Index Gradient," SPIE Paper 965-40, in *Current Developments in Optical Engineering III*, edited by R. E. Fischer and W. J. Smith, *SPIE Proceedings* **965**, 130–141 (1989).

15. G. H. Miley and P. E. Thiess, "A Unified Approach to Two-Region Ionization-Excitation Density Calculations," *Nucl. Appl.* **6**, 434–451 (1969).

16. J. C. Guyot, G. H. Miley, and J. T. Verdeyen, "Application of a Two-Region Heavy Charged Particle Model to Noble-Gas Plasmas Induced by Nuclear Radiations," *Nucl. Sci. Eng.* **48**, 373–386 (1972).

17. A. K. Chung and M. A. Prelas, "The Transport of Heavy Charged Particles in a Cylindrical Nuclear-Pumped Plasma," *Nucl. Sci. Eng.* **86**, 267–274 (1984).

18. J. R. Torczynski, "On the Motion of a Gas Experiencing Range-Dependent Volumetric Heating," *J. Fluid Mech.* **201**, 167–188 (1989).

19. J. R. Torczynski, "Heat-Transfer Regimes in Nuclear-Reactor-Pumped Gas Lasers," in *Proceedings of the 5th AIAA/ASME Thermophysics and Heat Transfer Conference*, submitted (1990).

20. R. G. Rehm and H. R. Baum, "The Equations of Motion for Thermally Driven, Buoyant Flows," *J. Res. Nat. Bur. Stand.* **83** (3), 297–308 (1978).

21. S. Paolucci, *On the Filtering of Sound from the Navier-Stokes Equations*, Sandia Report SAND82–8257, Sandia National Laboratories (1982).

22. J. R. Torczynski, "Partial Acoustic Filtering Applied to the Equations of Compressible Flow," in *Proceedings of the International Symposium on Nonsteady Fluid Dynamics*, submitted (1990).

23. J. R. Torczynski, "The Damping of Density Perturbations in Nuclear-Reactor-Pumped Lasers," *Nucl. Sci. Eng.*, submitted (1990).

24. R. C. Reid, J. M. Prausnitz, and B. C. Poling, *The Properties of Gases and Liquids* (McGraw-Hill, New York, 1986), pp. 514–518, 530–531.

Appendix

The equations describing the one-dimensional motion of a perfect gas can be acoustically filtered if the acoustic timescale is much smaller than other relevant timescales so that the Mach number of the induced flow is small.[18–22] Let the gas have a density field ρ, a pressure field p, a temperature field T, an energy field (per unit mass) e, a velocity field u, a specific heat ratio γ, temperature-dependent[24] shear and bulk viscosities μ and μ_v, and temperature-dependent[24] thermal conductivity k. Confine the gas between two side walls separated by a distance L, and heat the gas with the power density field Q. The gas motion is described by the perfect-gas equation of state and the conservation equations for mass, momentum, and energy:

$$p = R\rho T = (\gamma - 1)\rho e \ , \tag{A1}$$

$$\frac{\partial \rho}{\partial t} + \frac{\partial}{\partial x}\rho u = 0 \ , \tag{A2}$$

$$\frac{\partial}{\partial t}\rho u + \frac{\partial}{\partial x}\rho u^2 + \frac{\partial p}{\partial x} = \frac{\partial}{\partial x}\left[\left(\tfrac{4}{3}\mu + \mu_v\right)\frac{\partial u}{\partial x}\right] \ , \tag{A3}$$

$$\frac{\partial}{\partial t}\rho\left(e + \tfrac{1}{2}u^2\right) + \frac{\partial}{\partial x}\rho u\left(e + p/\rho + \tfrac{1}{2}u^2\right) = Q + \frac{\partial}{\partial x}\left(k\frac{\partial T}{\partial x}\right) + \frac{\partial}{\partial x}\left[u\left(\tfrac{4}{3}\mu + \mu_v\right)\frac{\partial u}{\partial x}\right] \ . \tag{A4}$$

Acoustic filtering is accomplished in the following manner. The gas pressure p is partitioned into two terms: $\bar{p}$, the average pressure in the x-direction; and $\hat{p} = p - \bar{p}$, the deviation from the average. Since the acoustic timescale is very small, it is not possible to build up

large pressure gradients, so $\hat{p}$ is always very small compared to $\bar{p}$. Inserting the expansion $p = \bar{p} + \hat{p}$ into the equations of motion, neglecting small terms, and performing averaging yields the following set of equations:[18-22]

$$\frac{\partial \rho}{\partial t} + \frac{\partial}{\partial x}\rho u = 0 \ , \tag{A5}$$

$$\frac{\partial}{\partial t}\rho u + \frac{\partial}{\partial x}\rho u^2 + \frac{\partial \hat{p}}{\partial x} = \frac{\partial}{\partial x}\left[\left(\tfrac{4}{3}\mu + \mu_v\right)\frac{\partial u}{\partial x}\right] \ , \tag{A6}$$

$$\frac{d\bar{p}}{dt} = (\gamma - 1)\left[\bar{Q} + \overline{\frac{\partial}{\partial x}\left(k\frac{\partial T}{\partial x}\right)}\right] \ , \tag{A7}$$

$$\gamma \bar{p}\frac{\partial u}{\partial x} = (\gamma - 1)\left[\hat{Q} + \widehat{\frac{\partial}{\partial x}\left(k\frac{\partial T}{\partial x}\right)}\right] \ , \tag{A8}$$

$$\overline{(\cdot)} = L^{-1}\int_0^L (\cdot)\, dx \ , \qquad \widehat{(\cdot)} = (\cdot) - \overline{(\cdot)} \ . \tag{A9}$$

Equations (A5) and (A6) are the conservation equations for mass and momentum, respectively. The pressure term in the momentum equation incorporates $\hat{p}$ since $\bar{p}$ is a function of time alone by virtue of averaging. Note that $\hat{p}$ appears only in Equation (A6), so this equation needs to be solved only for times at which knowledge of $\hat{p}$ is desired. Equation (A7) shows that the mean pressure rise is determined by the total average heat addition (fission-fragment heating and thermal-conduction loss) and as such is the ideal gas law in an unusual form. Equation (A8) determines the gas velocity in terms of the excess heating. If the sum of the excess fission-fragment heating and the excess thermal-conduction loss is positive, then $\partial u/\partial x$ is positive and the flow is locally expansive: gas is transported away from points with heating that is larger than average. If the sum of the excess fission-fragment heating and the excess thermal-conduction loss is negative, then $\partial u/\partial x$ is negative and the flow is locally compressive: gas is transported toward points with heating that is smaller than average.